CMS Physics Analysis Summary

Contact: cms-pag-conveners-susy@cern.ch 2016/08/04

An inclusive search for new phenomena in final states with one or more jets and missing transverse momentum at $\sqrt{s} = 13\,\text{TeV}$ with the α_T variable

The CMS Collaboration

Abstract

A search for new-physics phenomena is performed in final states containing one or more jets and an imbalance in transverse momentum in pp collisions at a centre-of-mass energy of 13 TeV. The analysed data sample, recorded with the CMS detector in 2016 at the CERN Large Hadron Collider, corresponds to an integrated luminosity of $12.9\,\text{fb}^{-1}$. Several kinematic variables are employed to strongly suppress the dominant background, multijet production from quantum chromodynamics, as well as discriminate effectively between other standard model and new-physics processes. The search provides sensitivity to a broad range of new-physics models that yield a stable weakly interacting massive particle. The observed candidate events are found to agree with the expected contributions from standard model processes. The result is interpreted in the mass parameter space of simplified supersymmetric models that assume the gluino-mediated and direct production of pairs of third-generation squarks. The gluino mass, and bottom and top squark masses, are excluded up to 1775, 1025, and 875 GeV, respectively.

1 Introduction

Supersymmetry (SUSY) [1–8] provides a complete, renormalisable extension to the standard model (SM) that can provide a solution to the hierarchy problem of the SM Higgs boson [9, 10] if SUSY is realised at the TeV scale. Further, the assumption of R-parity conservation [11] has important consequences for collider phenomenology and cosmology. Supersymmetric particles (sparticles) such as gluinos and squarks are expected to be produced in pairs at the LHC and promptly decay to SM particles and the lightest stable supersymmetric particle (LSP), which is generally assumed to be a weakly interacting, massive neutralino ($\widetilde{\chi}^0$) and a dark matter candidate. The characteristic signature of SUSY production at the LHC is a final state of multijets accompanied by significant missing transverse momentum, $\vec{p}_{\mathrm{T}}^{\,\mathrm{miss}}$.

The new energy frontier of the LHC during Run 2 provides a unique opportunity to search for the characteristic signatures of TeV-scale sparticles [12–15]. This Physics Analysis Summary presents an inclusive search for the pair production of massive coloured sparticles in hadronic final states with one or more energetic jets and missing transverse momentum, performed in pp collisions at a centre-of-mass energy $\sqrt{s} = 13\,\mathrm{TeV}$. The analysed data sample corresponds to an integrated luminosity of $12.9 \pm 0.8\,\mathrm{fb}^{-1}$ [16] collected by the Compact Muon Solenoid (CMS) experiment in 2016. A detailed description of the CMS detector can be found in Ref. [17]. Previous iterations of this search have been performed in pp collisions at $\sqrt{s} = 7$ [18–20], 8 [21, 22], and 13 TeV [23].

The search strategy is based around two key aspects in order to achieve a robust, inclusive search capable of exploiting the potential of the new LHC energy frontier under the challenging conditions of new beam and detector configurations early in Run 2. First, multiple tight selection criteria are employed to suppress multijet production, a manifestation of quantum chromodynamics (QCD), to a negligible level relative to all other SM background processes. Second, the experimental acceptance to a potential signal is maximised through the use of trigger conditions that maintain the same low thresholds employed during Run 1.

The strategy is built around the use of the kinematic variable α_{T} [18, 24], which provides powerful discrimination against multijet production. The α_{T} variable is constructed from jet-based quantities to provide robust discriminating power between sources of genuine and misreconstructed $\vec{p}_{\mathrm{T}}^{\,\mathrm{miss}}$, making it suitable for early searches operating at new energy and luminosity frontiers. Further variables are also employed to discriminate against multijet production and suppress this background process to a negligible level. The $\Delta\phi^*_{\mathrm{min}}$ [18] variable exploits azimuthal angular information and also provides strong rejection power against multijet events, including rare energetic events in which neutrinos carry a significant fraction of a jet's energy due to semileptonic decays of heavy-flavour mesons. The α_{T} variable is also utilised as part of the trigger conditions, providing high performance in terms of maintaining low thresholds for a given trigger bandwidth.

The search is based on an examination of the number of reconstructed jets per event, the number of these jets identified as originating from bottom quarks (b-tagged jets), and the scalar and vector sums of transverse momenta of these jets. These discriminating variables provide sensitivity to the different production mechanisms of massive coloured sparticles at hadron colliders (i.e. squark-squark, squark-gluino, and gluino-gluino), third-generation squark signatures, and a large range of mass splittings between the parent sparticle and the LSP. Interpretations of the result are provided in the parameter space of simplified models [25–27] that represent the gluino-mediated or direct pair production of third-generation squarks, and their subsequent decay to SM particles and the $\widetilde{\chi}^0$.

2 Event simulation

The search relies on several event samples, recorded by the CMS experiment or simulated with Monte Carlo (MC) generator programs, to estimate the contributions from SM backgrounds, as described in Section 3. The dominant SM backgrounds for the search are QCD multijet production and the associated production of jets and an top-antitop quark pair ($\mathrm{t\bar{t}}$), a single top quark, or a vector boson ($\mathrm{W} \to \ell\nu$, $\mathrm{Z} \to \nu\bar{\nu}$). Residual contributions from other processes, such as WW, WZ, ZZ (diboson) production and the associated production of $\mathrm{t\bar{t}}$ and a vector boson ($\mathrm{t\bar{t}W}$ and $\mathrm{t\bar{t}Z}$), are also considered. Other processes, such as Drell-Yan ($\mathrm{q\bar{q}} \to \mathrm{Z}/\gamma^* \to \ell^+\ell^-$) and γ + jets production, are also relevant for some control regions, defined below.

The MADGRAPH 5 aMC@NLO 2.2.2 [28] event generator is used at leading order (LO) accuracy to produce samples of W + jets, Z + jets, γ + jets, $\mathrm{t\bar{t}}$, and multijet events. The same generator is used at next-to-leading order (NLO) accuracy to generate samples of s-channel production of single top, as well as $\mathrm{t\bar{t}W}$ and $\mathrm{t\bar{t}Z}$ events. The NLO POWHEG v2 [29, 30] generator is used to describe the t- and tW-channel production of events containing single top quarks. The PYTHIA 8.2 [31] program is used to generate diboson (WW, WZ, ZZ) production. The simulated samples are normalised according to production cross sections that are calculated with NLO and next-to-NLO precision [28, 30, 32–36]. The description of the detector response, for these SM processes, is implemented using the GEANT4 [37] package.

Event samples for signal models involving the gluino-mediated or direct pair production of squarks, in association with up to two additional partons, are generated at leading order with MADGRAPH 5 aMC@NLO, and the decay of the sparticles is performed with PYTHIA 8.2 [31]. Inclusive, process-dependent, signal production cross sections are calculated with NLO plus next-to-leading-logarithm (NLL) accuracy [38–43]. The detector response is provided by the CMS fast simulation package [44].

The NNPDF3.0 LO and NNPDF3.0 NLO [45] parton distribution functions (PDF) are used, respectively, with the LO and NLO generators described above. The PYTHIA 8.2 [31] program is used to describe parton showering and hadronisation for all simulated samples. To model the effects of multiple pp collisions within the same or neighboring bunch crossings (pileup), all simulated events are generated with a nominal distribution of pp interactions per bunch crossing and then reweighted to match the pileup distribution as measured in data.

3 Event reconstruction and selections

Global event reconstruction is provided by the particle-flow (PF) algorithm [46, 47], which aims to identify single candidate particles using an optimized combination of information from all detector systems. In this process, the identification of the particle type (photon, electron, muon, charged hadron, neutral hadron) plays an important role in the determination of the particle direction and energy.

In order to suppress SM processes with genuine $\vec{p}_{\mathrm{T}}^{\,\mathrm{miss}}$ from neutrinos and select only multijet final states, events containing an isolated electron [48] or muon [49] with $p_{\mathrm{T}} > 10\,\mathrm{GeV}$ or isolated photon [50] with $p_{\mathrm{T}} > 25\,\mathrm{GeV}$ are vetoed. Furthermore, events containing an isolated track with $p_{\mathrm{T}} > 10\,\mathrm{GeV}$ are also vetoed in order to reduce the background contribution from final states containing hadronically-decaying tau leptons. Jets are reconstructed from candidate particles clustered by the anti-k_{T} algorithm [51] with a size parameter of 0.4. The jet energies are corrected to account for the effects of pileup and to establish a uniform relative response in η and a calibrated absolute response in transverse momentum p_{T} [52]. Jets considered in the

Table 1: Summary of the event selection requirements and categorisations used to define the signal region and control samples.

Baseline selection	
$E_{\mathrm{T}}^{\mathrm{miss}}$ cleaning	Filters related to beam and instrumental effects
Lepton/photon vetoes	$p_{\mathrm{T}} > 10$, 10, 25 GeV for isolated tracks, leptons, photons (respectively) and $\lvert\eta\rvert < 2.5$
Jet j_{i} acceptance	Consider each jet j_{i} that satisfies ${p_{\mathrm{T}}}^{j_{\mathrm{i}}} > 40$ GeV and $\lvert{\eta}^{j_{\mathrm{i}}}\rvert < 3$
Jet j_1 acceptance	${p_{\mathrm{T}}}^{j_1} > 100$ GeV and $\lvert{\eta}^{j_1}\rvert < 2.5$
Jet j_2 acceptance	${p_{\mathrm{T}}}^{j_2} < 40$ GeV (monojet), $40 < {p_{\mathrm{T}}}^{j_2} < 100$ GeV (asymmetric), ${p_{\mathrm{T}}}^{j_2} > 100$ GeV (symmetric)
Forward jet veto	Veto events containing jet satisfying $p_{\mathrm{T}} > 40$ GeV and $\lvert\eta\rvert > 3$
Jets below threshold	$H_{\mathrm{T}}^{\mathrm{miss}} / E_{\mathrm{T}}^{\mathrm{miss}} < 1.25$
Energy sums	$H_{\mathrm{T}} > 200$ GeV and $H_{\mathrm{T}}^{\mathrm{miss}} > 130$ GeV
Event categorisation	
n_{jet}	1 (monojet); 2, 3, 4, $\geq$5 (asymmetric); 2, 3, 4, $\geq$5 (symmetric)
n_{b}	0, 1, 2, $\geq$3 ($n_{\mathrm{b}} \leq n_{\mathrm{jet}}$)
H_{T} (GeV)	200, 250, 300, 350, 400, 500, 600, >800 GeV (some bins are dropped/merged *vs.* n_{jet})
Signal region (SR)	Baseline selection +
QCD multijet rejection	$\alpha_{\mathrm{T}} > 0.65$, 0.60, 0.55, 0.53, 0.52, 0.52, 0.52 (mapped to H_{T} bins in range 200–800 GeV)
QCD multijet rejection	$\Delta\phi^{*}_{\mathrm{min}} > 0.5$
Control samples (CS)	Baseline selection +
Multijet-enriched	SR + $H_{\mathrm{T}}^{\mathrm{miss}} / E_{\mathrm{T}}^{\mathrm{miss}} > 1.25$ (inverted)
γ + jets	1γ with $p_{\mathrm{T}} > 200$ GeV, $\lvert\eta\rvert < 1.45$, $\Delta R(\gamma, j_{\mathrm{i}}) > 1.0$, $H_{\mathrm{T}} > 400$ GeV, same α_{T} req. as SR
μ + jets	1μ with $p_{\mathrm{T}} > 30$ GeV, $\lvert\eta\rvert < 2.1$, $\Delta R(\mu, j_{\mathrm{i}}) > 0.5$, $30 < m_{\mathrm{T}}(\vec{p}_{\mathrm{T}}^{\,\mu}, \vec{p}_{\mathrm{T}}^{\,\mathrm{miss}}) < 125$ GeV
$\mu\mu$ + jets	2μ with $p_{\mathrm{T}} > 30$ GeV, $\lvert\eta\rvert < 2.1$, $\Delta R(\mu_{1,2}, j_{\mathrm{i}}) > 0.5$, $\lvert m_{\mu\mu} - m_{\mathrm{Z}}\rvert < 25$ GeV

analysis are required to have a transverse momentum above 40 GeV and $\lvert\eta\rvert < 3$.

The mass scale of the physics processes being probed is characterised by the scalar sum of the transverse momenta p_{T} of these jets, defined as $H_{\mathrm{T}} = \sum_{i=1}^{N_{\mathrm{jet}}} {p_{\mathrm{T}}}^{j_{\mathrm{i}}}$, where N_{jet} is the number of jets within the experimental acceptance. The missing transverse momentum vector $\vec{p}_{\mathrm{T}}^{\,\mathrm{miss}}$ is defined as the projection on the plane perpendicular to the beams of the negative vector sum of the momenta of all candidate particles in an event. Its magnitude is referred to as $E_{\mathrm{T}}^{\mathrm{miss}}$. The estimator for $E_{\mathrm{T}}^{\mathrm{miss}}$ used by this search is given by the magnitude of the vector sum of the transverse momenta of these jets, $H_{\mathrm{T}}^{\mathrm{miss}} = \lvert\sum_{i=1}^{N_{\mathrm{jet}}} \vec{p}_{\mathrm{T}}^{\,j_{\mathrm{i}}}\rvert$. Events are vetoed if any additional jet satisfies $p_{\mathrm{T}} > 40$ GeV and $\lvert\eta\rvert > 3$, in order to maintain the performance of the variable $H_{\mathrm{T}}^{\mathrm{miss}}$ as an estimator of $E_{\mathrm{T}}^{\mathrm{miss}}$. Significant hadronic activity and $\vec{p}_{\mathrm{T}}^{\,\mathrm{miss}}$ in the event is ensured by requiring $H_{\mathrm{T}} > 200$ GeV and $H_{\mathrm{T}}^{\mathrm{miss}} > 130$ GeV, respectively. The most energetic jet in the event is required to satisfy $p_{\mathrm{T}} > 100$ GeV.

A number of beam- and detector-related effects can lead to events with large values of $E_{\mathrm{T}}^{\mathrm{miss}}$, such as beam halo, reconstruction failures, spurious detector noise, or event misreconstruction due to detector inefficiencies. These events, with large, non-physical values of $E_{\mathrm{T}}^{\mathrm{miss}}$, are rejected with high efficiency by applying a range of dedicated vetoes [21, 53]. An additional dedicated veto is employed to deal with the circumstance in which several jets with transverse momentum below the p_{T} thresholds and collinear in ϕ can result in significant $H_{\mathrm{T}}^{\mathrm{miss}}$ relative to $E_{\mathrm{T}}^{\mathrm{miss}}$, the latter of which is less sensitive to jet thresholds. This type of background, typical of multijet events, is suppressed while maintaining high efficiency for SM or new physics processes with significant $\vec{p}_{\mathrm{T}}^{\,\mathrm{miss}}$ by requiring $H_{\mathrm{T}}^{\mathrm{miss}} / E_{\mathrm{T}}^{\mathrm{miss}} < 1.25$.

The aforementioned selection requirements define a baseline set, as summarised in Table 1. Additional requirements, described below, are utilised to define a sample of candidate signal

events, labelled henceforth as the signal region. Four additional control samples of events are employed to estimate the background contributions from SM processes, which modify and expand on the baseline selection requirements. The first control sample is enriched in multijet events and is used to estimate the multijet contribution in the signal region. Three additional control samples comprising γ + jets, μ + jets, or $\mu\mu$ + jets events, defined by the baseline set of selections and the inversion of one of the photon or lepton vetoes, are used to estimate background contributions from SM processes, predominantly W($\to \ell\nu$) + jets, Z($\to \nu\bar{\nu}$) + jets, and $\mathrm{t\bar{t}}$ production, that lead to final states containing jets and significant $\vec{p}_{\mathrm{T}}^{\,\mathrm{miss}}$. Additional kinematic requirements are employed to ensure the control samples are enriched in the same SM processes that contribute to background events in the signal region, and are depleted in contributions from multijet production or a wide variety of SUSY models (i.e. so-called signal contamination). The control samples are defined such that the kinematic properties of events in the control regions and the candidate signal events resemble as closely as possible one another, once the photon, muon, or dimuon system is ignored in the calculation of quantities such as H_{T} and $H_{\mathrm{T}}^{\mathrm{miss}}$. The event selection requirements for the four control samples are summarised in Table 1.

Events containing at least two jets are categorised according to *symmetric* or *asymmetric* topologies if the second-most energetic jet satisfies, respectively, $p_{\mathrm{T}} > 100\,\mathrm{GeV}$ or $40 < p_{\mathrm{T}} < 100\,\mathrm{GeV}$. Events that contain only one jet satisfying the requirement $p_{\mathrm{T}} > 40\,\mathrm{GeV}$ are categorised as a *monojet* topology. The symmetric topology targets the pair production of sparticles and their cascade decays, while the monojet and asymmetric topologies target nearly mass-degenerate SUSY models, as well as the direct production of weakly interacting massive particles. Events are further categorised according to the number of jets per event (n_{jet}), the number of reconstructed jets identified as originating from a b quark (n_{b}), and H_{T}. These categorisations, summarised in Table 1, are used identically for the signal region and the four control samples. Finally, the search exploits the use of the $H_{\mathrm{T}}^{\mathrm{miss}}$ variable as a discriminant between the dominant SM backgrounds and new-physics signatures. The expected distribution of events as a function of $H_{\mathrm{T}}^{\mathrm{miss}}$ is determined from simulation, an approach that is validated in multiple data control samples.

For events satisfying the baseline selections described above, summarised in Table 1, the multijet background dominates over all other SM backgrounds. The α_{T} kinematic variable, first introduced in Refs. [18, 24], is used to efficiently reject multijet events with transverse momentum mismeasurements while retaining sensitivity to new physics with genuine $\vec{p}_{\mathrm{T}}^{\,\mathrm{miss}}$ signatures. The variable α_{T} depends solely on the measurements of the transverse momenta and azimuthal angles of jets and it is intrinsically robust against the presence of jet energy mismeasurements in multijet systems. For dijet events, the α_{T} variable is defined as $\alpha_{\mathrm{T}} = p_{\mathrm{T}}^{\mathrm{j2}}/M_{\mathrm{T}}$ where $p_{\mathrm{T}}^{\mathrm{j2}}$ is the transverse momentum of the less-energetic jet, and M_{T} is the transverse mass of the dijet system. For a perfectly measured dijet event with $p_{\mathrm{T}}^{\mathrm{j1}} = p_{\mathrm{T}}^{\mathrm{j2}}$ and jets back-to-back in ϕ, and in the limit in which the momentum of each jet is large compared with its mass, the value of α_{T} is 0.5. For the case of an imbalance in the measured transverse momenta of back-to-back jets, α_{T} is reduced to a value smaller than 0.5, which gives the variable its intrinsic robustness. Values significantly greater than 0.5 are observed when the two jets are not back to back and are recoiling against significant, genuine $\vec{p}_{\mathrm{T}}^{\,\mathrm{miss}}$. The definition of the α_{T} variable can be generalised for events with two or more jets, as described in Ref. [21].

Multijet events typically populate the region $\alpha_{\mathrm{T}} \lesssim 0.5$ and the α_{T} distribution is characterised by a sharp edge at 0.5, beyond which the multijet event yield falls by several orders of magnitude. Multijet events with extremely rare but large stochastic fluctuations in the calorimetric measurements of jet energies can lead to values of α_{T} slightly above 0.5. The edge at 0.5 sharp-

ens with increasing H_T for multijet events, primarily due to a corresponding increase in the average jet energy and thus an improvement in the jet energy resolution, but also because the threshold effect of jets below the p_T threshold contributing significantly to H_T^{miss} decreases with increasing H_T. This motivates a H_T-dependent α_T requirement that varies in the range 0.52–0.65 for the region $H_T < 800\,GeV$.

The $\Delta\phi^*_{min}$ variable considers the minimum azimuthal angular separation of a jet and the H_T^{miss} vector derived from all other jets in the event. The $\Delta\phi^*_{min}$ variable provides powerful discriminating power between final states with genuine $\vec{p}_T^{miss}$ and mismeasured QCD multijet events. The variable is also highly efficient at suppressing any potential contribution from rare energetic multijet events that yield high jet multiplicities and significant E_T^{miss} due to high-multiplicity neutrino production in semileptonic heavy-flavour decays. The neutrinos are typically collinear with respect to the axis of a jet and carry a significant fraction of the energy. The requirement $\Delta\phi^*_{min} > 0.5$ is sufficient to suppress effectively the multijet background. For the region $H_T < 800\,GeV$, the requirements on both the α_T and $\Delta\phi^*_{min}$ variables are utilised, whereas for the region $H_T > 800\,GeV$, the necessary control of the QCD multijet background is achieved solely with the $\Delta\phi^*_{min}$ requirement.

The tight requirements on the variables α_T, $\Delta\phi^*_{min}$, and H_T^{miss}/E_T^{miss} suppress the expected contribution from multijet events to the percent level with respect to the total expected background counts from other SM processes, for all bins of the signal region. Further, control variables are inspected to provide confidence that any multijet contamination due to instrumental effects is negligible. The aforementioned requirements complete the definition of the signal region, and are summarised in Table 1.

The categorisation of candidate signal events, as a function of n_{jet}, n_b, H_T, and H_T^{miss}, and the number of bins within the signal region are determined primarily by the statistical power of the multiple data control samples. The signal region and control samples cover a large phase space, defined primarily by the loose requirements $H_T > 200\,GeV$ and $H_T^{miss} > 130\,GeV$, and candidate signal events are categorised into 194 exclusive sub-regions according to n_{jet}, n_b, and H_T. Within each sub-region, events are further categorised according to H_T^{miss}: the first bin is defined by the range $130 < H_T^{miss} < 200\,GeV$, subsequent bins have a width of 100 GeV, up to a final open bin that satisfies $H_T^{miss} > 800\,GeV$. If the statistical power of the simulated or data control samples is limited, the higher H_T^{miss} bins are merged, reducing the threshold on the final open bin, to the limiting case of a single open bin defined by $H_T^{miss} > 130\,GeV$. This procedure ensures the information taken from simulation is always adequately supported by checks in the data control samples. On average, less than four bins in H_T^{miss} are utilised per (n_{jet}, n_b, H_T) category.

Candidate signal events are recorded with multiple jet-based trigger conditions that require both H_T and α_T to satisfy predetermined thresholds. In addition, a trigger condition based solely on H_T is used to record candidate events for the region $H_T > 800\,GeV$. A dedicated trigger condition requiring the presence of significant H_T^{miss} and E_T^{miss} is used to record events containing one or more jets. The trigger-level jet energies are corrected to account for energy scale and pileup effects. The trigger strategy provides efficiencies at or near 100% for all bins of the signal region.

4 Estimation of the QCD multijet background

Potential contamination from multijet events in the signal region is estimated by exploiting the ratio of multijet events that satisfy or fail the requirement $H_T^{miss}/E_T^{miss} < 1.25$, as deter-

mined from simulation, for events categorised according to n_{jet} and H_{T}. Estimates of the QCD multijet background counts are determined in a data sideband, defined by the requirement $H_{\mathrm{T}}^{\mathrm{miss}}/E_{\mathrm{T}}^{\mathrm{miss}} > 1.25$, by correcting the observed counts in data to account for contamination from non-multijet backgrounds (vector boson and $\mathrm{t\bar{t}}$ production, plus residual contributions from other SM processes). The products of the corrected counts and ratios provide independent estimates of the multijet background as a function of n_{jet} and H_{T}.

The multijet background estimates are found to be typically at the percent level relative to the sum of all other SM backgrounds, in all bins of the signal region. The distribution of these small contributions as a function of n_{b} and $H_{\mathrm{T}}^{\mathrm{miss}}$ is determined from simulation. Statistical uncertainties associated with the finite event counts in data and simulated samples are propagated to each estimate. The uncertainties in the estimates of the contamination from non-multijet backgrounds in the $H_{\mathrm{T}}^{\mathrm{miss}}/E_{\mathrm{T}}^{\mathrm{miss}}$ data sideband are determined according to the prescription described in Section 5. Finally, the ratios determined from simulated events are validated in a further multijet-enriched data sideband, defined by $\Delta\phi_{\mathrm{min}}^{*} < 0.5$, from which a systematic uncertainty of 100% is determined.

5 Estimation of SM backgrounds with genuine $\vec{p}_{\mathrm{T}}^{\,\mathrm{miss}}$

Following the suppression of multijet events, the background counts in the signal region mainly arise from SM processes that produce neutrinos, resulting in final states with significant $\vec{p}_{\mathrm{T}}^{\,\mathrm{miss}}$. In events with low counts of jets and b quark jets, the largest backgrounds with genuine $\vec{p}_{\mathrm{T}}^{\,\mathrm{miss}}$ are from the associated production of W or Z bosons with jets, followed by either the weak decays $\mathrm{Z} \to \nu\bar{\nu}$ or $\mathrm{W} \to \tau\nu$, where the τ decays hadronically and is identified as a jet; or by leptonic decays that are not rejected by the dedicated electron or muon vetoes. The veto of events containing isolated tracks is efficient at further suppressing these backgrounds as well as the single-prong hadronic decay of the tau lepton. At higher jet and b-tag multiplicities, top quark production followed by semileptonic weak top quark decay becomes important.

The simulated samples of γ + jets, $\mathrm{W}(\to \ell\nu)$ + jets, $\mathrm{Z}(\to \ell\ell)$ + jets, and $\mathrm{t\bar{t}}$ production are normalised to data using scale factors derived in data sidebands, enriched in the relevant process. The definition of the sidebands, the selection applied and the scale factors are listed in Table 2. These factors are derived after all other corrections are applied to the simulated samples.

Table 2: Cross section corrections for SM processes determined from data sidebands.

SM process	Control sample	Data sideband	Corrrection
γ + jets	γ + jets	$0.50 < \alpha_{\mathrm{T}} < 0.52$	1.33 ± 0.03
$\mathrm{W}(\to \ell\nu)$ + jets	μ + jets	$100 < H_{\mathrm{T}}^{\mathrm{miss}} < 130\,\mathrm{GeV}$	1.13 ± 0.01
$\mathrm{Z}(\to \ell\ell)$ + jets	$\mu\mu$ + jets	$100 < H_{\mathrm{T}}^{\mathrm{miss}} < 130\,\mathrm{GeV}$	0.99 ± 0.02
$\mathrm{t\bar{t}}$	μ + jets, $\mu\mu$ + jets	$100 < H_{\mathrm{T}}^{\mathrm{miss}} < 130\,\mathrm{GeV}$	0.86 ± 0.01

The method to estimate the non-multijet backgrounds in the signal region relies on the use of transfer factors, which are constructed per bin (in terms of n_{jet}, n_{b}, and H_{T}) per data control sample. The transfer factors are determined from the simulated event samples and are ratios of expected yields in the corresponding bins of the signal region and control samples. The transfer factors are used to extrapolate from the event yields measured in data control samples to an expectation for the total background event yields in the signal region. Three disjoint data control samples, binned identically to the signal region, are used to estimate the contributions from the non-multijet SM background processes, as summarised in Table 1.

The μ + jets sample is recorded using a trigger condition that requires an isolated muon and

the event selection criteria are chosen in order to ensure high trigger efficiency. Furthermore, the muon is required to be well separated from the jets in the event and the transverse mass (m_{T}) of the muon and $\vec{p}_{\mathrm{T}}^{\,\mathrm{miss}}$ system must satisfy $30 < m_{\mathrm{T}}(\vec{p}_{\mathrm{T}}^{\,\mu}, \vec{p}_{\mathrm{T}}^{\,\mathrm{miss}}) < 125\,\mathrm{GeV}$ to ensure a sample rich in W bosons (produced promptly or from the decay of top quarks). The $\mu\mu$ + jets sample uses similar selection criteria as the μ + jets sample and the same trigger condition. Exactly two oppositely-charged, isolated muons are required, the muons must be distanced from the jets in the event, and the invariant mass of the dimuon system ($m_{\mu\mu}$) must be within a window of $\pm 25\,\mathrm{GeV}$ around the mass of the Z boson, $|m_{\mu\mu} - m_{\mathrm{Z}}| < 25\,\mathrm{GeV}$. For both the muon and dimuon samples, no requirement is made on the variable α_{T} in order to increase the statistical precision of the predictions derived from these samples, in contrast to the identical α_{T} requirements made for the signal region and photon control sample. The γ + jets sample is recorded using a single photon trigger condition. The event selection criteria comprise an isolated photon with $E_{\mathrm{T}} > 200\,\mathrm{GeV}$ and $H_{\mathrm{T}} > 400\,\mathrm{GeV}$.

Three independent estimates of the irreducible background of $\mathrm{Z} \to \nu\bar{\nu}$ + jets events are determined from the γ + jets, $\mu\mu$ + jets, and μ + jets data control samples. The γ + jets and $\mathrm{Z} \to \mu\mu$ + jets processes have similar kinematic properties when the photon or muons are ignored [54], albeit different acceptances. In addition, the γ + jets process has a larger production cross section than $\mathrm{Z} \to \nu\bar{\nu}$ + jets events. The μ + jets data sample is used to provide an estimate for the $\mathrm{Z} \to \nu\bar{\nu}$ + jets contribution as well as the other dominant SM processes, $\mathrm{t\bar{t}}$ and W boson production. Residual background contributions from processes such as single-top-quark, diboson, and Drell-Yan production are also included.

Table 3: Systematic uncertainties in the transfer factors used in the method to estimate the SM backgrounds with genuine $\vec{p}_{\mathrm{T}}^{\,\mathrm{miss}}$ in the signal region. The quoted ranges provide the minimum and maximum values used across all bins in n_{jet} and H_{T}.

Systematic source	Uncertainty in transfer factor [%]			
	$\mu + jets \Rightarrow \mathrm{t\bar{t}/W}$	$\mu + jets \Rightarrow \mathrm{Z} \to \nu\bar{\nu}$	$\mu\mu + jets \Rightarrow \mathrm{Z} \to \nu\bar{\nu}$	$\gamma + jets \Rightarrow \mathrm{Z} \to \nu\bar{\nu}$
Corrections applied to simulation:				
Jet energy scale	1–5	1–5	1–5	1–5
b-tag efficiency / mistag	1–5	1–5	1–5	1–5
Lepton scale factors	1–3	1–3	1–3	-
Pileup	0–2	0–2	0–2	0–2
Signal trigger efficiency	1–2	1–2	1–2	1–2
Muon trigger efficiency	2	2	2	-
Photon trigger efficiency	-	-	-	1–2
Top quark p_{T}	1–10	1–30	1–10	-
Derived from closure tests in data:				
W/Z ratio	-	4–15	-	-
Z/γ ratio	-	-	-	6–11
$\mathrm{W/t\bar{t}}$ composition	4–30	-	-	-
W polarisation	2–10	2–10	-	-
$\alpha_{\mathrm{T}}/\ \Delta\phi^{*}_{\mathrm{min}}$	3–30	3–30	3–30	-

Several sources of uncertainty in the transfer factors are evaluated. The most relevant effects are discussed below, and generally fall into one of two categories. The first category concerns uncertainties in "scale factor" corrections applied to simulation, which are determined using inclusive data samples that are defined by loose selection criteria, to account for the mismodelling of theoretical and experimental parameters. The second category concerns "closure tests" in data that probe various aspects of the accuracy of the simulation to model correctly the transfer factors in the phase space of this search.

The uncertainties in the transfer factors are studied for variations in scale factors related to: the

jet energy scale, the efficiency and misidentification probability of b quark jets, the efficiency to identify or veto well-reconstructed, isolated leptons, and the modelling of the transverse momentum of top quarks. A 5% uncertainty in the minimum bias cross section is assumed and propagated through to the reweighting procedure to account for differences between the simulated and data-derived measurements of the pileup distributions. Uncertainties in the trigger efficiency measurements are also propagated to the transfer factors. The aforementioned systematic uncertainties, resulting from variations in scale factors, are summarised in Table 3, along with representative magnitudes. Each source of uncertainty is assumed to vary with a fully correlated behaviour across the full phase space of the signal and control regions.

Sources of additional uncertainty are determined from sets of "closure tests" based on data control samples [21]. Each set uses the observed event counts in up to eight bins in H_{T} for each of the nine n_{jet} event categories in one of the three independent data control samples, along with the corresponding transfer factors determined from simulation, to obtain a prediction of the observed yields in another control sample (or, in one case, n_{b} event category). Each set of tests is designed to target a specific (potential) source of bias in the simulation modelling that may introduce an n_{jet}- or H_{T}-dependent source of systematic bias in the transfer factors [21]. Several sets of tests are performed. The Z/γ ratio determined from simulation is tested against the same ratio measured using $\mathrm{Z}(\rightarrow \mu\mu)$ + jets events and the γ + jets sample. The W/Z ratio is also probed using the μ + jets and $\mu\mu$ + jets samples. A further set probes the modelling of the relative composition between $\mathrm{W}(\rightarrow \ell\nu)$ + jets and $\mathrm{t\bar{t}}$ events using μ + jets events containing exactly zero or one more b-tagged jets, which represents a larger extrapolation in relative composition than used in the search. The effects of W polarisation are probed by using μ + jets events with a positively charged muon to predict those containing a negatively charged muon. Finally, the accuracy of the modelling of the efficiencies of the α_{T} and $\Delta\phi^{*}_{\mathrm{min}}$ requirements are estimated using the μ + jets sample.

For each set of tests, the level of closure, which considers only statistical uncertainties, is inspected to ensure no statistically significant biases are observed as a function of the nine n_{jet} categories or the eight H_{T} bins. In the absence of such a bias, the level of closure is recomputed by integrating over either all monojet and asymmetric topologies, or the symmetric n_{jet} categories. The level of closure and its statistical uncertainty are combined in quadrature to determine additional contributions to the uncertainties in the transfer factors. These uncertainties are considered to be fully correlated between the monojet and asymmetric topologies or the symmetric topology, and fully uncorrelated between these two regions in n_{jet} and H_{T} bins. If the closure tests use the $\mu\mu$ + jets sample, the level of closure is determined by additionally integrating over pairs of adjacent H_{T} bins. These uncertainties, derived from the closure tests in data, are summarised in Table 3, along with representative magnitudes. These uncertainties are the dominant contribution to the total uncertainty in the transfer factors, due to the limited number of events in the data control samples.

Templates determined from simulation are used to predict the background counts in the $H_{\mathrm{T}}^{\mathrm{miss}}$ dimension. Uncertainties in the scale factor corrections applied to simulated events, as discussed above in the context of transfer factors, are propagated as uncertainties in the $H_{\mathrm{T}}^{\mathrm{miss}}$ templates. Uncertainties in the trigger efficiency measurements are also propagated to the $H_{\mathrm{T}}^{\mathrm{miss}}$ templates. These sources of uncertainty are assumed to vary with a correlated behaviour across the full phase space of the signal region. Multiple data control samples are used to evaluate the degree to which the simulation describes the $H_{\mathrm{T}}^{\mathrm{miss}}$ distributions observed in data, and to assign appropriate systematic uncertainties, which can be significant ($\sim$50–100%) in the most sensitive $H_{\mathrm{T}}^{\mathrm{miss}}$ bins. The $H_{\mathrm{T}}^{\mathrm{miss}}$ templates from simulation are compared to the distributions observed in the control samples, and inspected for trends, by assuming a linear behaviour of the ratio of

observed and simulated counts as a function of H_T^{miss}. Linear fits are performed independently for each bin defined by n_{jet}, n_b, and H_T. No significant biases or trends are observed, given the statistical power of the control samples, and systematic uncertainties are determined from the constrained fit parameters. These uncertainties are treated as fully uncorrelated between bins defined in terms of n_{jet}, n_b, and H_T, and also with respect to the systematic uncertainties in the transfer factors, summarised in Table 3.

6 Results

A likelihood model of the observations in all data samples is used to obtain a consistent prediction of the SM backgrounds and to test for the presence of a variety of signal models. In each bin of H_T for events in the same category of n_{jet} and n_b, the observation is modelled as a Poisson-distributed variable around the sum of the SM expectation (and a potential signal contribution). The SM expectation is related to the expected yields in the μ + jets, $\mu\mu$ + jets, and γ + jets control samples via transfer factors derived from simulation. Likelihood functions describe the yields in the H_T bins of the μ + jets, $\mu\mu$ + jets, and γ + jets control samples in the same category of n_{jet} and n_b as the signal region. The systematic uncertainties summarised in Table 3 are accommodated in the likelihood function by nuisance parameters, the measurements of which are assumed to follow a gaussian distribution.

The expected number of events from SM processes is determined from a simultaneous fit to data in the three control regions ("CR-only fit"), as well as a fit including the signal region ("full fit"). The likelihood function is maximised over all fit parameters under the SM-only hypothesis. Figures 1–3 summarise, respectively, the observed number of candidate signal events and the SM expectations from the CR-only fit, in the monojet, asymmetric, and symmetric topologies. No significant tension is observed between the predictions and data in the signal region, which is well described by the SM-only hypothesis.

Figure 4 shows the distributions of observed counts in data and expected counts from SM background processes as a function of the H_T^{miss} variable for two event categories, defined by high n_{jet}, high H_T, and $n_b = 0$ or $n_b \geq 3$, which are expected to provide sensitivity to models with TeV-scale gluinos.

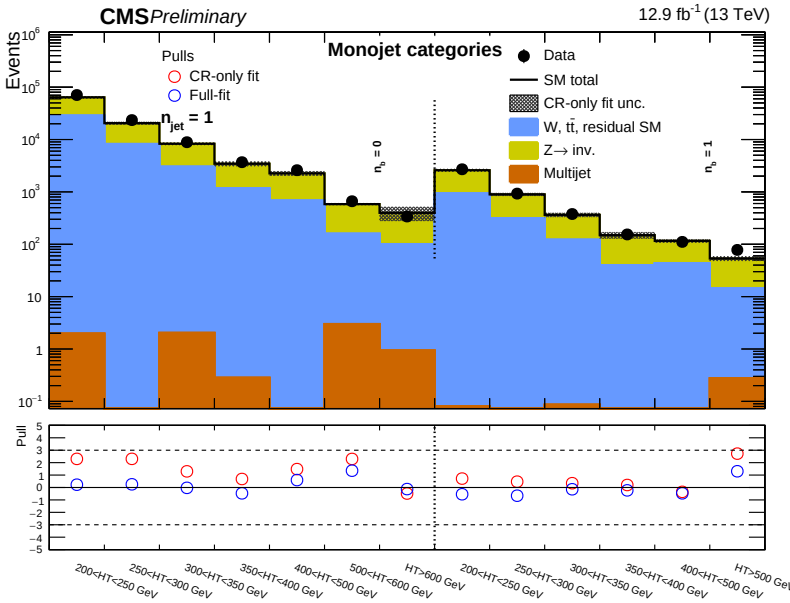

Figure 1: (Top panel) Event yields observed in data (solid circles) and SM expectations with their associated uncertainties (black histogram with shaded band) from a CR-only fit as a function of n_{b} and H_{T} for the monojet topology ($n_{\mathrm{jet}} = 1$) in the signal region. (Bottom panel). The significance of deviations (pulls) observed in data with respect to the SM expectations from the CR-only (red circles) and full fit (blue circles). The pulls are indicative only and cannot be considered independently.

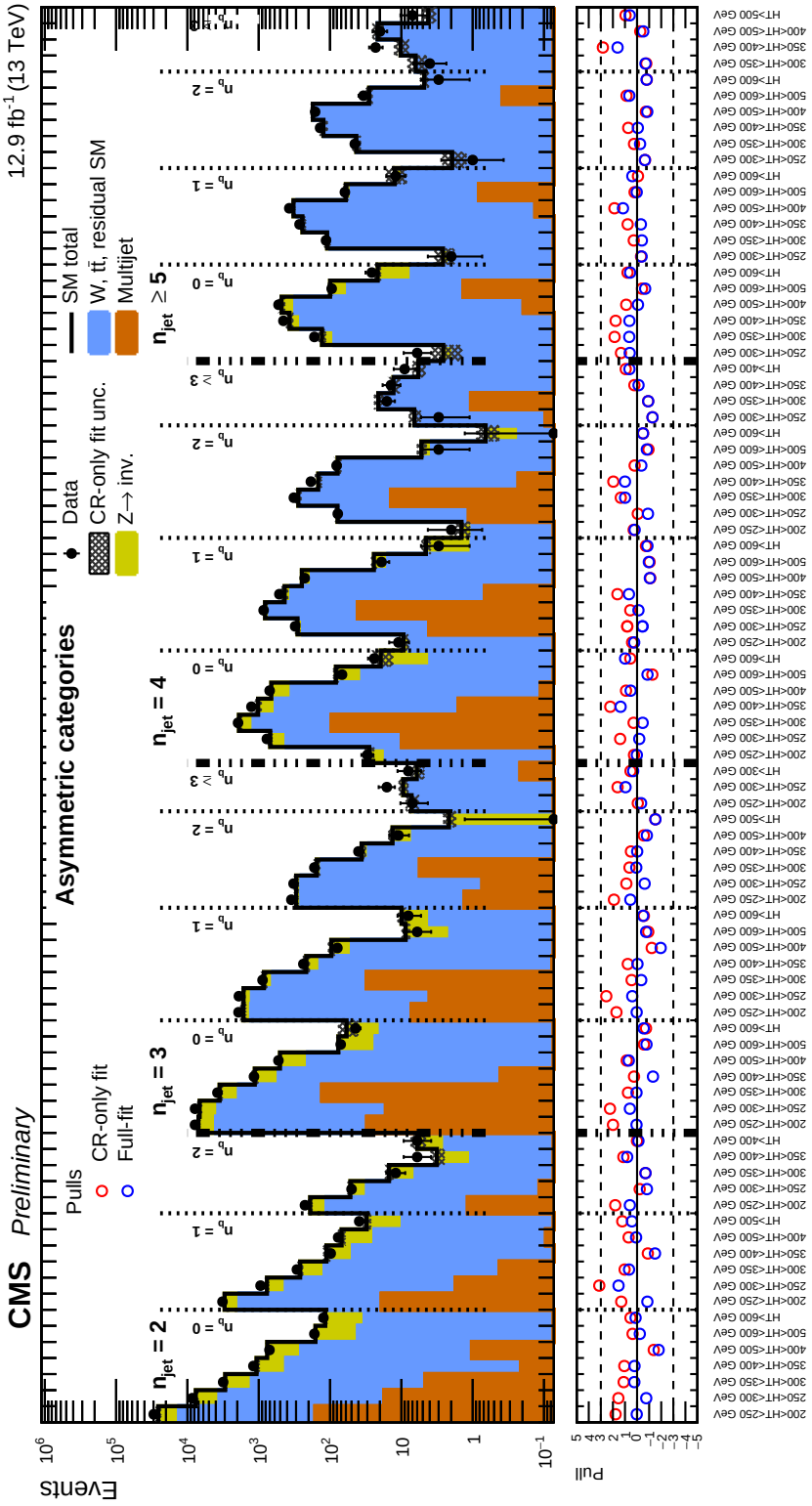

Figure 2: (Top panel) Event yields observed in data (solid circles) and SM expectations with their associated uncertainties (black histogram with shaded band) from a CR-only fit, integrated over $H_{\mathrm{T}}^{\mathrm{miss}}$, as a function of n_{jet}, n_{b}, and H_{T} for the asymmetric topology in the signal region. (Bottom panel). The significance of deviations (pulls) observed in data with respect to the SM expectations from the CR-only (red circles) and full fit (blue circles). The pulls are indicative only and cannot be considered independently.

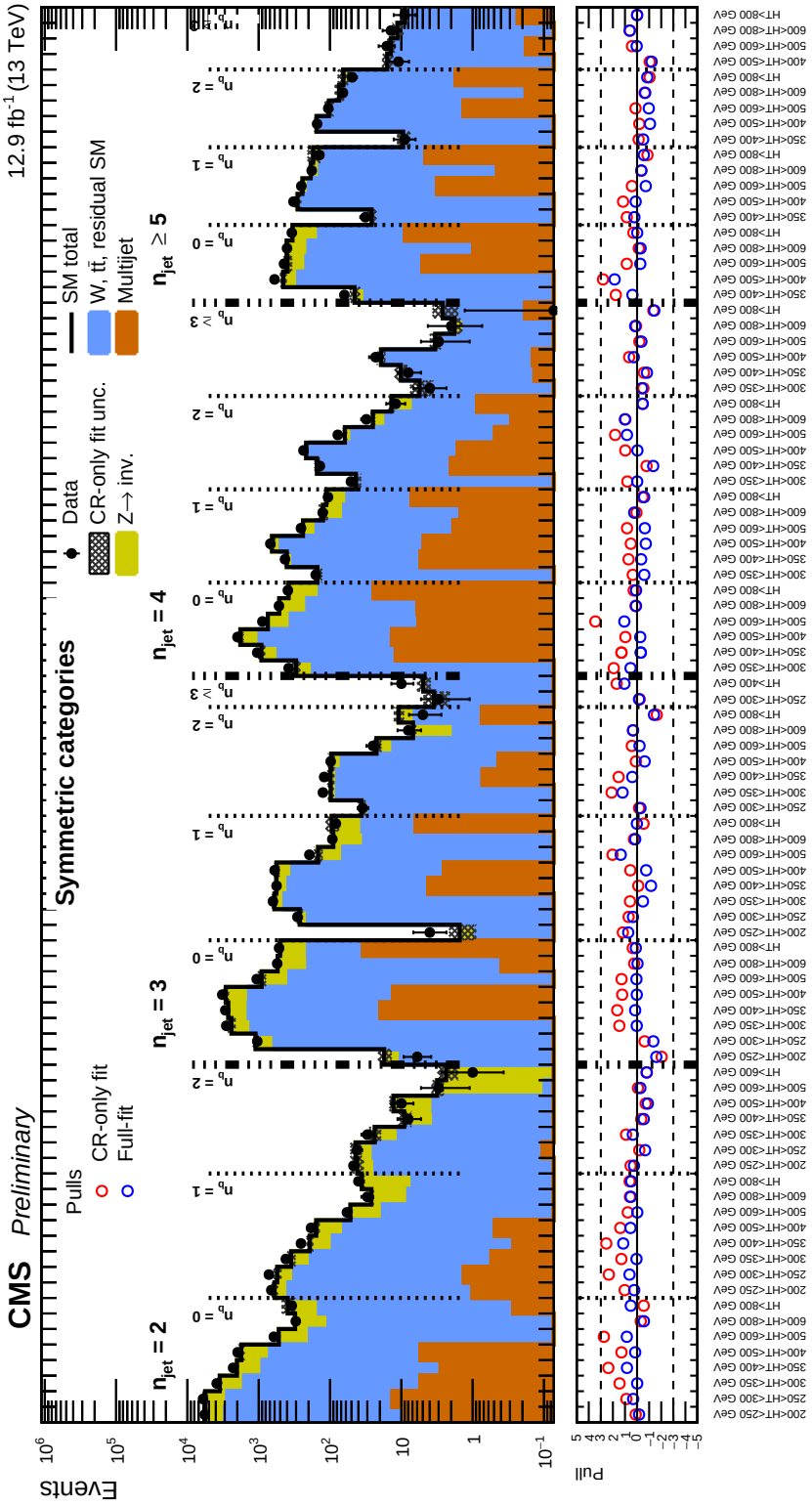

Figure 3: (Top panel) Event yields observed in data (solid circles) and SM expectations with their associated uncertainties (black histogram with shaded band) from a CR-only fit, integrated over $H_{\mathrm{T}}^{\mathrm{miss}}$, as a function of n_{jet}, n_{b}, and H_{T} for the symmetric topology in the signal region. (Bottom panel). The significance of deviations (pulls) observed in data with respect to the SM expectations from the CR-only (red circles) and full fit (blue circles). The pulls are indicative only and cannot be considered independently.

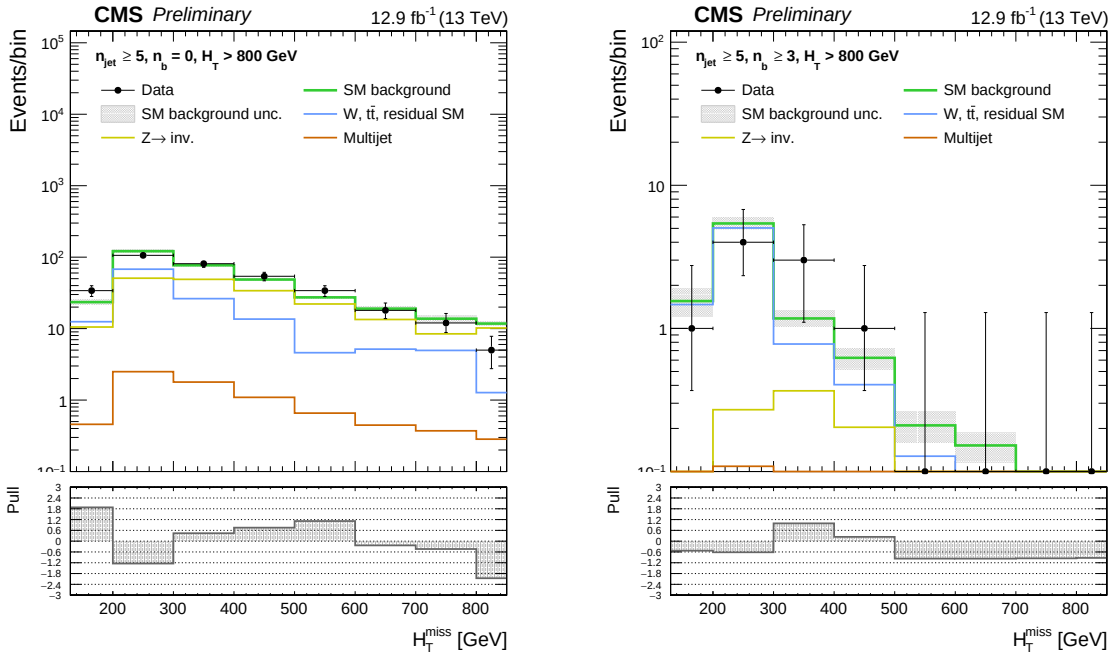

Figure 4: Event yields observed in data (solid circles) and SM expectations from the CR-only fit with their associated uncertainties (green histogram with shaded band) as a function of $H_{\mathrm{T}}^{\mathrm{miss}}$ for events in the signal region that satisfy $n_{\mathrm{jet}} \geq 5$, $H_{\mathrm{T}} > 800\,\mathrm{GeV}$, and (Left) $n_{\mathrm{b}} = 0$ or (Right) $n_{\mathrm{b}} \geq 3$. The final bin is the overflow bin. The bottom panels indicate the significance of the deviations (pulls) observed in data with respect to the SM expectations, expressed in terms of the total uncertainty in the SM expectations. The pulls are indicative only and cannot be considered independently.

7 Interpretation

The results of the search are used to constrain the parameter space of simplified supersymmetric models [25–27]. Each model represents a unique production and decay mode (i.e. 100% branching ratio). The gluino-mediated or direct production of third-generation squark pairs, and the decay of of each squark to SM particles and the $\widetilde{\chi}^0$, are considered. All other sparticles are assumed to be too heavy to be produced directly. In the case of gluino pair production, three-body decays of the gluinos are assumed via off-shell squarks.

Under the background + signal hypothesis, and in the presence of a non-zero signal contribution, a modified frequentist approach is used to determine upper limits at 95% confidence level (CL) on the cross section, σ_{UL} (pb), to produce pairs of supersymmetric particles as a function of the parent sparticle and the LSP masses. The potential contributions from a new-physics signal to each of the signal and control regions are considered, even though the only significant contribution occurs in the signal region and not the control region (i.e. signal contamination). The approach is based on the one-sided (LHC-style) profile likelihood ratio as the test statistic, the CL_s criterion [55, 56], and asymptotic formulae [57] are utilised to approximate the distributions of the test statistics under the SM background-only and signal + background hypotheses.

The experimental acceptance times efficiency ($\mathcal{A} \times \varepsilon$) and its uncertainty are evaluated independently for each model as a function of the gluino or squark mass and the $\widetilde{\chi}^0$ mass. Several sources to the uncertainty in $\mathcal{A} \times \varepsilon$ are considered. The effect of each source of uncertainty on the $H_{\mathrm{T}}^{\mathrm{miss}}$ templates is evaluated from simulated signal events, categorised according to n_{jet}, n_{b}, and H_{T}. Correlations are taken into account where appropriate, including those relevant to signal contamination that may contribute to counts in the control samples.

Table 4: Representative magnitudes of systematic uncertainties in the experimental acceptance for simplified models that assume the pair production of bottom squarks and their decay to a b quark and a $\widetilde{\chi}^0$.

Systematic source	Type	Correlated	Typical magnitude (%)
Luminosity	Normalisation	Yes	6.2
Monte Carlo statistics	Norm. + shape	No	1–50
Jet energy scale	Norm. + shape	Yes	3–10
b-tag efficiency scale factors	Norm. + shape	Yes	5–40
Lepton scale factors	Normalisation	Yes	1–5
Pile-up	Norm. + shape	Yes	0–5
Trigger efficiency	Norm. + shape	Yes	0–4
Initial state radiation	Norm. + shape	Yes	1–20
Modelling of $H_{\mathrm{T}}^{\mathrm{miss}}$	Normalisation	Yes	1–5

The magnitude of each contribution depends on the model and the masses of the parent sparticle and LSP. The following sources of uncertainty are dominant: the statistical uncertainty arising from the finite size of simulated signal samples, the modelling of initial-state radiation (ISR), corrections to the jet energy scale evaluated in simulation, and the modelling of scale factors applied to simulated event samples that correct for differences in the efficiency and misidentification probability for b-tagged jets. The choice of PDF set, or variations therein, predominantly affects $\mathcal{A} \times \varepsilon$ through changes in the p_{T} spectrum of the system recoil, which is covered by the ISR uncertainty, hence no additional uncertainty is adopted. Uncertainties in $\mathcal{A} \times \varepsilon$ due to variations in the renormalisation and factorisation scales are determined to be relatively small. In both cases, contributions to the uncertainty in the theory production cross section are considered. The uncertainty in the integrated luminosity is assumed to be 6.2%. Representative values of the dominant systematic uncertainties are summarised in Table 4.

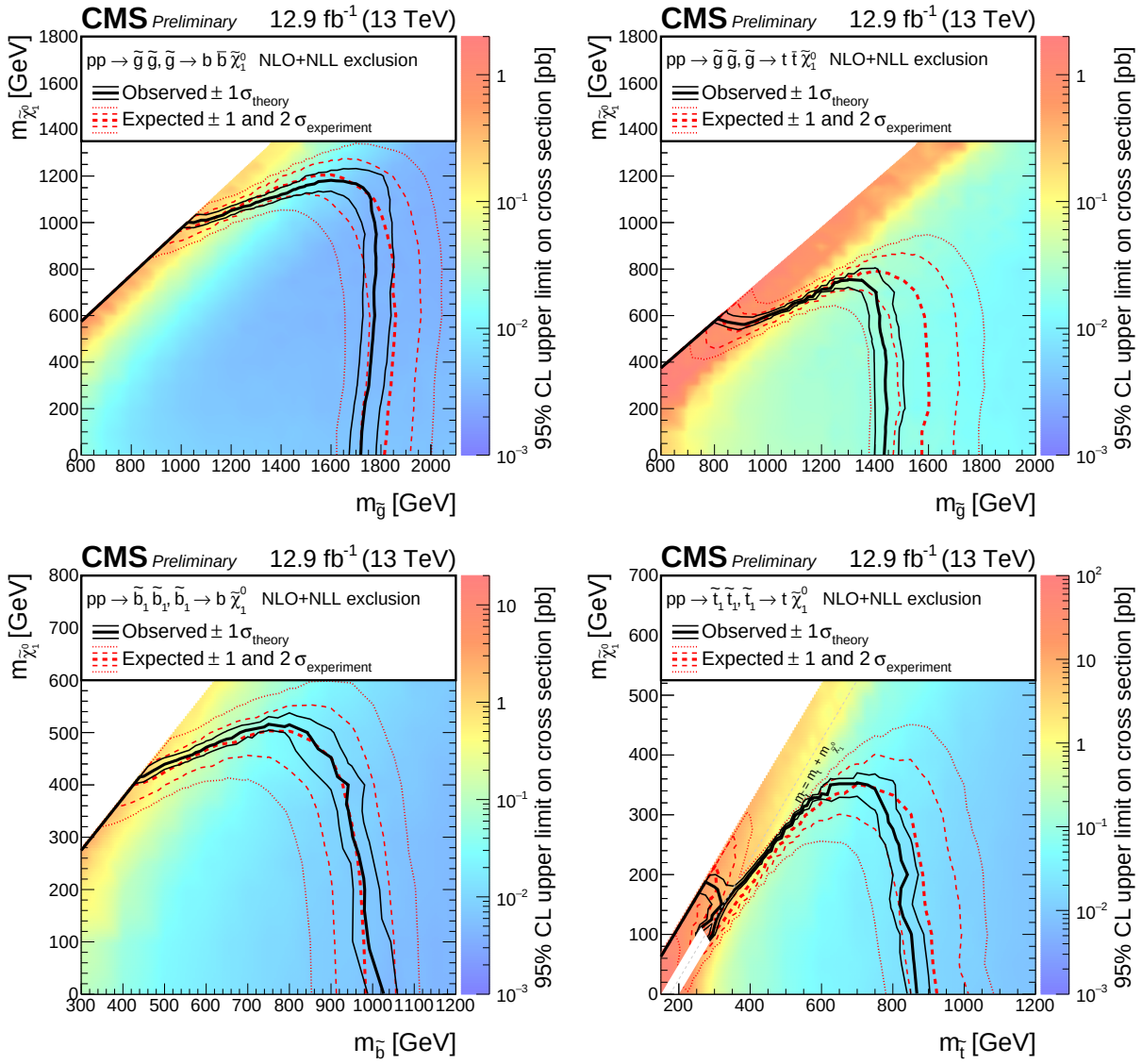

Figure 5: Observed upper limit in cross section at 95% confidence level (indicated by the colour scale) for simplified models that assume the (Top) gluino-mediated or (Bottom) direct production of (Left) bottom or (Right) top squark pairs, as a function of the gluino or squark mass and the $\tilde{\chi}_1^0$ mass. The black solid thick (thin) line indicates the observed mass exclusion regions assuming the nominal ($\pm 1\sigma$ theory uncertainty) production cross section. The red dashed thick (thin) line indicates the median ($\pm 1\sigma$ experimental uncertainty) expected mass exclusion regions.

Table 5: Summary of the mass limits obtained for the four classes of simplified models. The limits indicate the strongest observed (expected) mass exclusions for the gluino or squarks, and $\widetilde{\chi}_1^0$, and the quoted values have uncertainties of ± 25 GeV.

Production mode	Squark	Strongest obs. (exp.) mass exclusion [GeV]	
		Gluino or squark	$\widetilde{\chi}^0$
Gluino-mediated	Bottom	1775 (1850)	1175 (1200)
Gluino-mediated	Top	1450 (1600)	750 (800)
Direct	Bottom	1025 (975)	525 (500)
Direct	Top	875 (925)	350 (350)

Figure 5 shows the observed upper limit on the production cross section at 95% confidence level as a function of the gluino or squark and $\widetilde{\chi}^0$ masses for models that assume the gluino-mediated or direct production of bottom and top squark pairs. Also shown are the observed mass exclusion regions when varying the production cross section by its theoretical uncertainty, and the expected mass exclusion regions with the ± 1 and ± 2 standard-deviation variations.

The search places stringent limits in the mass parameter space of these models, with observed exclusions in gluino and $\widetilde{\chi}^0$ masses as high as 1775 and 1175 GeV, respectively. In the case of direct production of bottom squarks, masses as high as 1025 and 525 GeV are excluded. Finally, top squark and $\widetilde{\chi}^0$ masses up to 875 and 350 GeV are excluded. A summary of the limits is provided in Table 5.

8 Summary

An inclusive search for supersymmetry with the CMS experiment is reported, based on a data sample of pp collisions collected in 2016 at $\sqrt{s} = 13$ TeV, corresponding to an integrated luminosity of $12.9 \pm 0.8\,\text{fb}^{-1}$. Final states with jets and significant $\vec{p}_{\mathrm{T}}^{\,\mathrm{miss}}$, as expected from the production and decay of massive gluinos and squarks, have been analysed. Candidate signal events are categorised according to the number of reconstructed jets, the number of jets identified to originate from bottom quarks, and the scalar and vector sums of the transverse momentum of jets. The sum of standard model backgrounds per bin has been estimated from a simultaneous binned likelihood fit to event yields in the signal region and control samples. The observed yields in the signal region are found to be in agreement with the expected contributions from standard model processes.

Limits are determined in the mass parameter space of simplified models involving the gluino-mediated and direct production of third-generation squark pairs. The excluded mass parameter space extends significantly beyond that set by previous searches, with observed exclusions in gluino mass, and bottom and top squark masses, as high as 1775, 1025, and 875 GeV, respectively.

References

[1] Y. A. Gol'fand and E. P. Likhtman, "Extension of the Algebra of Poincaré Group Generators and Violation of p Invariance", *JETP Lett.* **13** (1971) 323.

[2] J. Wess and B. Zumino, "Supergauge transformations in four dimensions", *Nucl. Phys. B* **70** (1974) 39, doi:10.1016/0550-3213(74)90355-1.

[3] H. P. Nilles, "Supersymmetry, Supergravity and Particle Physics", *Phys. Reports* **110** (1984) 1, doi:10.1016/0370-1573(84)90008-5.

[4] H. Haber and G. Kane, "The Search for Supersymmetry: Probing Physics Beyond the Standard Model", *Phys. Reports* **117** (1987) 75, doi:10.1016/0370-1573(85)90051-1.

[5] R. Barbieri, S. Ferrara, and C. A. Savoy, "Gauge Models with Spontaneously Broken Local Supersymmetry", *Phys. Lett. B* **119** (1982) 343, doi:10.1016/0370-2693(82)90685-2.

[6] S. Dawson, E. Eichten, and C. Quigg, "Search for Supersymmetric Particles in Hadron - Hadron Collisions", *Phys. Rev. D* **31** (1985) 1581, doi:10.1103/PhysRevD.31.1581.

[7] E. Witten, "Dynamical Breaking of Supersymmetry", *Nucl. Phys. B* **188** (1981) 513, doi:10.1016/0550-3213(81)90006-7.

[8] S. Dimopoulos and H. Georgi, "Softly Broken Supersymmetry and SU(5)", *Nucl. Phys. B* **193** (1981) 150, doi:10.1016/0550-3213(81)90522-8.

[9] ATLAS Collaboration, "Observation of a new particle in the search for the Standard Model Higgs boson with the ATLAS detector at the LHC", *Phys. Lett. B* **716** (2012) 1, doi:10.1016/j.physletb.2012.08.020.

[10] CMS Collaboration, "Observation of a new boson at a mass of 125 GeV with the CMS experiment at the LHC", *Phys. Lett. B* **716** (2012) 30, doi:10.1016/j.physletb.2012.08.021.

[11] G. R. Farrar and P. Fayet, "Phenomenology of the Production, Decay, and Detection of New Hadronic States Associated with Supersymmetry", *Phys. Lett. B* **76** (1978) 575, doi:10.1016/0370-2693(78)90858-4.

[12] ATLAS Collaboration, "Search for new phenomena in final states with large jet multiplicities and missing transverse momentum with ATLAS using $\sqrt{s} = 13$ TeV proton–proton collisions", (2016). arXiv:1602.09058. Accepted by *Phys. Lett. B*.

[13] ATLAS Collaboration, "Search for new phenomena in final states with an energetic jet and large missing transverse momentum in pp collisions at $\sqrt{s} = 13$ TeV using the ATLAS detector", arXiv:1604.07773. Submitted to *Phys. Rev. D*.

[14] CMS Collaboration, "Search for supersymmetry in the multijet and missing transverse momentum final state in pp collisions at 13 TeV", (2016). arXiv:1602.06581. Accepted by *Phys. Lett. B*.

[15] CMS Collaboration, "Search for new physics with the M_{T2} variable in all-jets final states produced in pp collisions at $\sqrt{s} = 13$ TeV", (2016). arXiv:1603.04053. Submitted to *JHEP*.

[16] CMS Collaboration, "CMS Luminosity Based on Pixel Cluster Counting - Summer 2012 Update", CMS Physics Analysis Summary CMS-PAS-LUM-12-001, 2012.

[17] CMS Collaboration, "The CMS experiment at the CERN LHC", *JINST* **03** (2008) S08004, doi:10.1088/1748-0221/3/08/S08004.

[18] CMS Collaboration, "Search for Supersymmetry in pp Collisions at 7 TeV in Events with Jets and Missing Transverse Energy", *Phys. Lett. B* **698** (2011) 196, doi:10.1016/j.physletb.2011.03.021.

[19] CMS Collaboration, "Search for Supersymmetry at the LHC in Events with Jets and Missing Transverse Energy", *Phys. Rev. Lett.* **107** (2011) 221804, doi:10.1103/PhysRevLett.107.221804.

[20] CMS Collaboration, "Search for supersymmetery in final states with missing transverse energy and 0, 1, 2, or $\geq$3 b-quark jets in 7 TeV pp collisions using the α_{T} variable", *JHEP* **01** (2013) 077, doi:10.1007/JHEP01(2013)077.

[21] CMS Collaboration, "Search for supersymmetry in hadronic final states with missing transverse energy using the variables α_{T} and b-quark multiplicity in pp collisions at $\sqrt{s} = 8$ TeV", *EPJC* **01** (2013) 077, doi:10.1007/JHEP01(2013)077.

[22] CMS Collaboration, "Search for top squark pair production in compressed-mass-spectrum scenarios in proton-proton collisions at $\sqrt{s} = 8$ TeV using the α_{T} variable", (2016). arXiv:1605.08993. Submitted to *Phys. Lett. B*.

[23] CMS Collaboration, "Search for new physics in final states with jets and missing transverse momentum in $\sqrt{s} = 13$ TeV pp collisions with the α_T variable", (2015). CMS-PAS-SUS-15-005.

[24] L. Randall and D. Tucker-Smith, "Dijet Searches for Supersymmetry at the Large Hadron Collider", *Phys. Rev. Lett.* **101** (2008) 221803, doi:10.1103/PhysRevLett.101.221803.

[25] J. Alwall, P. Schuster, and N. Toro, "Simplified Models for a First Characterization of New Physics at the LHC", *Phys. Rev. D* **79** (2009) 075020, doi:10.1103/PhysRevD.79.075020.

[26] J. Alwall, M.-P. Le, M. Lisanti, and J. G. Wacker, "Model-independent jets plus missing energy searches", *Phys. Rev. D* **79** (2009) 015005, doi:10.1103/PhysRevD.79.015005.

[27] D. Alves et al., "Simplified models for LHC new physics searches", *J. Phys. G* **39** (2012) 105005, doi:10.1088/0954-3899/39/10/105005.

[28] J. Alwall et al., "The automated computation of tree-level and next-to-leading order differential cross sections, and their matching to parton shower simulations", *Journal of High Energy Physics* **07** (2014) 079, doi:10.1007/JHEP07(2014)079, arXiv:1405.0301.

[29] S. Alioli, P. Nason, C. Oleari, and E. Re, "A general framework for implementing NLO calculations in shower Monte Carlo programs: the POWHEG BOX", *JHEP* **06** (2010) 043, doi:10.1007/JHEP06(2010)043, arXiv:1002.2581.

[30] E. Re, "Single-top Wt-channel production matched with parton showers using the POWHEG method", *Eur. Phys. J. C* **71** (2011) 1547, doi:10.1140/epjc/s10052-011-1547-z, arXiv:1009.2450.

[31] T. Sjöstrand et al., "An Introduction to PYTHIA 8.2", *Comput. Phys. Commun.* **191** (2015) 159, doi:10.1016/j.cpc.2015.01.024, arXiv:1410.3012.

[32] R. Gavin, Y. Li, F. Petriello, and S. Quackenbush, "W Physics at the LHC with FEWZ 2.1", *Comput. Phys. Commun.* **184** (2013) 208, doi:10.1016/j.cpc.2012.09.005, arXiv:1201.5896.

[33] R. Gavin, Y. Li, F. Petriello, and S. Quackenbush, "FEWZ 2.0: A code for hadronic Z production at next-to-next-to-leading order", *Comput. Phys. Commun.* **182** (2011) 2388, doi:10.1016/j.cpc.2011.06.008, arXiv:1011.3540.

[34] T. Melia, P. Nason, R. Rontsch, and G. Zanderighi, "W^+W^-, WZ and ZZ production in the POWHEG BOX", *JHEP* **11** (2011) 078, doi:10.1007/JHEP11(2011)078, arXiv:1107.5051.

[35] C. M. and A. Mitov, "Top++: A program for the calculation of the top-pair cross-section at hadron colliders", *Comput. Phys. Commun.* **185** (2014) 2930, doi:10.1016/j.cpc.2014.06.021, arXiv:1112.5675.

[36] S. Alioli, P. Nason, C. Oleari, and E. Re, "NLO single-top production matched with shower in POWHEG: s- and t-channel contributions", *JHEP* **09** (2009) 111, doi:10.1088/1126-6708/2009/09/111, arXiv:0907.4076.

[37] S. Agostinelli et al., "GEANT4 — a simulation toolkit", *Nucl. Instr. and Meth. A* **506** (2003) 250, doi:10.1016/S0168-9002(03)01368-8.

[38] W. Beenakker, R. Höpker, M. Spira, and P. M. Zerwas, "Squark and gluino production at hadron colliders", *Nucl. Phys. B* **492** (1997) 51, doi:10.1016/S0550-3213(97)00084-9.

[39] A. Kulesza and L. Motyka, "Threshold Resummation for Squark-Antisquark and Gluino-Pair Production at the LHC", *Phys. Rev. Lett.* **102** (2009) 111802, doi:10.1103/PhysRevLett.102.111802.

[40] A. Kulesza and L. Motyka, "Soft gluon resummation for the production of gluino-gluino and squark-antisquark pairs at the LHC", *Phys. Rev. D* **80** (2009) 095004, doi:10.1103/PhysRevD.80.095004.

[41] W. Beenakker et al., "Soft-gluon resummation for squark and gluino hadroproduction", *JHEP* **09** (2009) 041, doi:10.1088/1126-6708/2009/12/041.

[42] W. Beenakker et al., "Squark and gluino hadroproduction", *Int. J. Mod. Phys. A* **26** (2011) 2637, doi:10.1142/S0217751X11053560.

[43] C. Borschensky et al., "Squark and gluino production cross sections in pp collisions at $\sqrt{s} = 13$, 14, 33 and 100 TeV", *Eur. Phys. J. C* **74** (2014) 3174, doi:10.1140/epjc/s10052-014-3174-y, arXiv:1407.5066.

[44] CMS Collaboration, "The fast simulation of the CMS detector at LHC", *J. Phys. Conf. Ser.* **331** (2011) 032049, doi:10.1088/1742-6596/331/3/032049.

[45] NNPDF Collaboration, "Parton distributions for the LHC Run II", *JHEP* **04** (2015) 040, doi:10.1007/JHEP04(2015)040, arXiv:1410.8849.

[46] CMS Collaboration, "Particle–Flow Event Reconstruction in CMS and Performance for Jets, Taus, and $E_{\mathrm{T}}^{\mathrm{miss}}$", CMS Physics Analysis Summary CMS-PAS-PFT-09-001, 2009.

[47] CMS Collaboration, "Commissioning of the particle-flow event reconstruction with the first LHC collisions recorded in the CMS detector", CMS Physics Analysis Summary CMS-PAS-PFT-10-001, 2010.

[48] CMS Collaboration, "Electron reconstruction and identification at $\sqrt{s}$ = 7 TeV", CMS Physics Analysis Summary EGM-10-004, 2010.

[49] CMS Collaboration, "Performance of CMS muon reconstruction in pp collision events at $\sqrt{s} = 7$ TeV", *JINST* **7** (2012) P10002, doi:10.1088/1748-0221/7/10/P10002.

[50] CMS Collaboration, "Isolated Photon Reconstruction and Identification at $\sqrt{s}$ = 7 TeV", CMS Physics Analysis Summary EGM-10-006, 2010.

[51] M. Cacciari, G. P. Salam, and G. Soyez, "The anti-k_{T} jet clustering algorithm", *JHEP* **04** (2008) 063, doi:10.1088/1126-6708/2008/04/063.

[52] CMS Collaboration, "Jet energy scale and resolution in the CMS experiment in pp collisions at 8 TeV", arXiv:1607.03663. Submitted to *JINST*.

[53] CMS Collaboration, "Performance of the CMS missing transverse momentum reconstruction in pp data at $\sqrt{s}$ = 8 TeV", *JINST* **10** (2015) P02006, doi:10.1088/1748-0221/10/02/P02006, arXiv:1411.0511.

[54] Z. Bern et al., "Driving Missing Data at Next-to-Leading Order", (2011). arXiv:1106.1423.

[55] T. Junk, "Confidence level computation for combining searches with small statistics", *Nucl. Instr. and Meth. A* **434** (1999) 435, doi:10.1016/S0168-9002(99)00498-2.

[56] A. L. Read, "Presentation of search results: the CL_s technique", *J. Phys. G* **28** (2002) 2693, doi:10.1088/0954-3899/28/10/313.

[57] G. Cowan, K. Cranmer, E. Gross, and O. Vitells, "Asymptotic formulae for likelihood-based tests of new physics", *Eur. Phys. J. C* **71** (2011) 1554, doi:10.1140/epjc/s10052-011-1554-0.